Available online at www.sciencedirect.com
ScienceDirect
Journal of the European Ceramic Society 30 (2010) 2569–2576
www.elsevier.com/locate/jeurceramsoc

Effect of microstructure on dielectric and fatigue strengths of $BaTiO_3$

Shih-Chun Lu [a], Yin-Hua Chen [a], Wei-Hsing Tuan [a,*], Jay Shieh [a], Chin-Yi Chen [b]

[a] *Department of Materials Science and Engineering, National Taiwan University, Taipei 106, Taiwan*
[b] *Department of Materials Science and Engineering, Feng-Chia University, Taichung 40724, Taiwan*

Received 29 October 2009; received in revised form 21 April 2010; accepted 23 April 2010
Available online 3 June 2010

Abstract

In the present study, bulk barium titanate ceramic specimens with bimodal microstructures are prepared and their dielectric and fatigue strengths under an alternating electric field are investigated. It is found that both the dielectric and fatigue strengths decrease with increasing amount of coarse grains. The scatter of the fatigue strength is characterized with the Weibull statistics. The extent of scatter of the fatigue strength data correlates strongly with the size distribution of the coarse grains. Such correlation is resulted from the presence of intrinsic defects within the microstructure. Direct microstructure evidences are provided.

Keywords: Dielectric properties; Fatigue; Barium titanate; Microstructure

1. Introduction

Barium titanate ($BaTiO_3$) is a ferroelectric ceramic with relatively high dielectric constant. The $BaTiO_3$-based oxides have been widely used as the dielectrics for ceramic capacitors.[1] Their potential to be utilized in non-volatile memory applications has also been suggested.[2] One major concern on the use of $BaTiO_3$ ceramics is their long-term reliability under the influence of alternating electric fields. The key parameters to ensure their reliability are the dielectric and fatigue strengths.

Due to the increasing demand on device miniaturization, the thickness of the dielectric layers in commercial passive and active components is rapidly decreasing. High dielectric strength has therefore become a vital characteristic in order to avoid unwanted electrical shortings. For ferroelectric materials, a substantial alternating electric field can induce domain switchings. Strains associated with the domain switchings could lead to fatigue cracking and subsequently degrade the dielectric, ferroelectric and mechanical properties of the materials. A considerable literature exists concerning the fatigue characteristics of ferroelectric ceramics, especially on subjects such as the governing parameters for fatigue cracking and the gradual degradation of bulk material properties throughout a cyclically loaded specimen.[3–11] In contrast, the effect of material makeup, such as the microstructure, on the fatigue strength of ferroelectric ceramics, has received relatively less attention. Furthermore, the correlation between the dielectric strength and fatigue strength has not yet been thoroughly addressed.

The microstructure of $BaTiO_3$ is sensitive to its composition, especially to the Ba/Ti ratio and the amount of impurity.[12] A slightly lower Ba/Ti ratio (<1.000) will induce the formation of a liquid phase above the eutectic temperature (1312 °C) of $BaTiO_3$–$Ba_6Ti_{17}O_{40}$.[12,13] The presence of the liquid phase could trigger the growth of abnormal grains. A bimodal grain size distribution is thus commonly observed in the Ti-rich $BaTiO_3$ specimens. Due to the anisotropic thermal expansion characteristics of $BaTiO_3$ crystals, stresses are induced during cooling through the Curie temperature. Depending on the grain size, the resultant residual stresses could initiate microcracks and spontaneous cracking.[14] The presence of abnormal grains has been related to the formation of intrinsic defects, such as microcracks, in the sintered ceramic specimens; such relationship has been investigated and confirmed by Tuan and Lin adopting a thermal expansion analysis.[15] In the present study, $BaTiO_3$ specimens with various amounts of abnormal grains are prepared and the effect of microstructure on the dielectric and

* Corresponding author. Tel.: +886 2 33663899; fax: +886 2 23659800.
E-mail address: tuan@ntu.edu.tw (W.-H. Tuan).

0955-2219/$ – see front matter © 2010 Elsevier Ltd. All rights reserved.
doi:10.1016/j.jeurceramsoc.2010.04.028

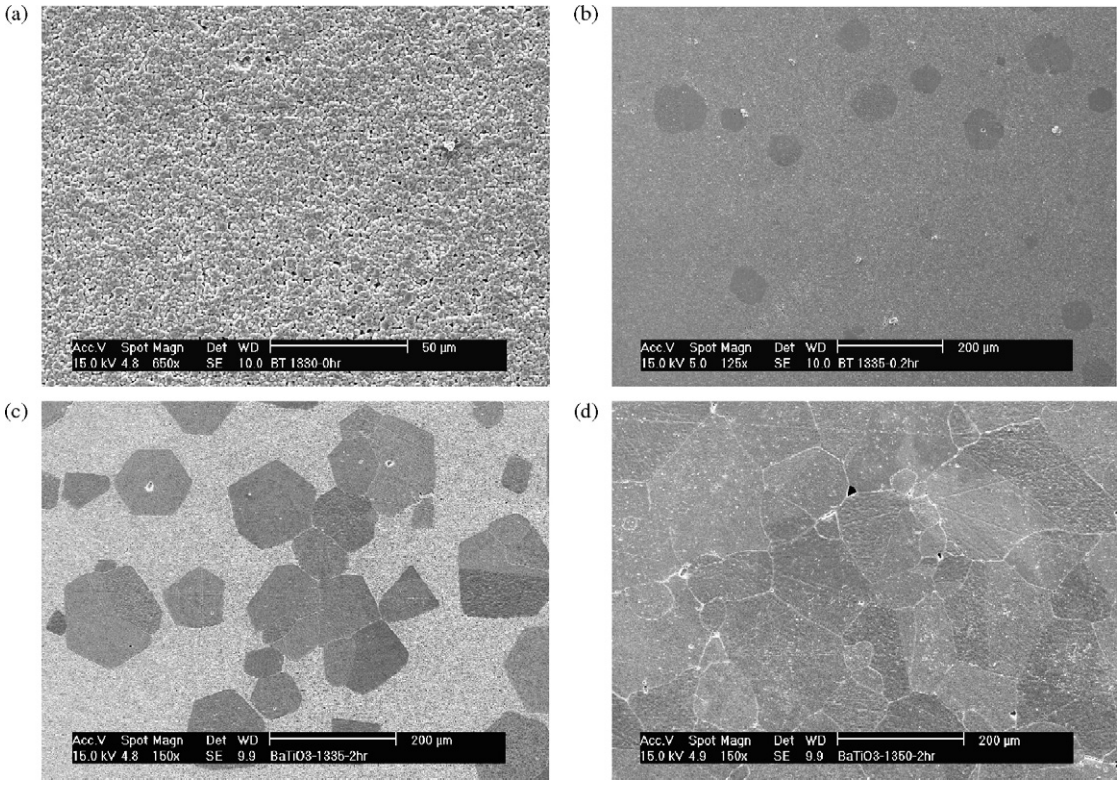

Fig. 1. SEM micrographs of $BaTiO_3$ specimens sintered at (a) 1330 °C for 0.1 h, (b) 1335 °C for 0.2 h, (c) 1335 °C for 2 h and (d) 1350 °C for 2 h.

fatigue strengths of the specimens under cyclic electric fields is investigated.

2. Experimental procedure

Detailed procedures for the preparation of $BaTiO_3$ specimens with various amounts of abnormal grains are documented in a previous study.[16] A brief description is given here. A commercial $BaTiO_3$ powder (NEB, Ferro Co., Inc., OH, USA) with a reported Ba/Ti ratio of 1.000 ± 0.002 was used as the raw material. The powder was ball-milled in ethyl alcohol for 4 h. The grinding media used were zirconia balls. After drying and sieving, the $BaTiO_3$ powder was die-pressed uniaxially into discs with a diameter of 10 mm at 25 MPa. The green compacts were then buried in a pure zirconia powder and sintered in a covered alumina crucible. In order to prepare the specimens with various amounts of abnormal grains, the sintering procedure was carried out at four different conditions: 1330 °C for 0.1 h, 1335 °C for 0.2 h, 1335 °C for 2 h and 1350 °C for 2 h. The heating and cooling rates were set at 5 °C/min.

Crystalline phases of the sintered $BaTiO_3$ specimens were confirmed using X-ray diffractometry (XRD; PW1830, Philips, The Netherlands) with Cu Kα radiation. Densities of the sintered specimens were determined by the Archimedes' method. Polishing and etching steps were carried out for the observation of microstructures. The cross-section surfaces of the specimens were ground and polished with diamond pastes first. The microstructural features at the polished cross-section surfaces were revealed by thermal etching at 1260 °C for 0.5 h and then observed using optical microscopy and scanning electron microscopy (SEM; XL30, Philips, The Netherlands). The sizes of the grains were determined by sketching the grain boundaries from the SEM micrographs. The area of each grain was determined by an image analysis technique. By assuming each grain had a spherical shape, the grain diameter could be determined from the grain area. In order to estimate the grain size distribution, more than 1200 grains were counted for each sintering condition.

For electric field-induced fatigue measurements, the $BaTiO_3$ specimens were ground to a thickness of about 250 μm. In order to avoid premature arcing failure due to surface roughness under electrical loading, all surfaces of the specimens were polished down to 1 μm finish before carrying out fatigue measurements. Silver-based pastes (D-2864, Shoei Chemical, Inc., Japan) were fired (600 °C for 1 h in air) onto the circular faces of the specimens to form the top and bottom electrodes. The dielectric hysteresis curves (electric displacement D vs. electric field E) of the specimens were determined by a ferroelectric analyzer (TF2000, aixACCT, Germany). The cyclic electric fields used for fatigue testing were supplied by a high-voltage amplifier. From the high-voltage source, a bipolar cyclic voltage of sinusoidal waveform at a frequency of 60 Hz was applied to each $BaTiO_3$ specimen, producing an alternating electric field parallel to the thickness direction of the specimen. The magnitude of the electric field was 1.8 kV/mm. The entire electrical loading fixture was supported in a silicon oil bath to prevent breakdown arcing. The fatigue test was terminated when the resistivity of the specimen decreased below 10^6 Ω cm (corresponds to a leakage current > 5 mA).

Table 1
Microstructure characteristics of $BaTiO_3$ specimens prepared under various sintering conditions.

Sintering temperature (°C)/dwell time (h)	Relative density (%)	Area fraction of abnormal grains (%)	Size of abnormal grains (μm)	Size of normal grains (μm)
1330/0.1	93.9	0	–	1.6 ± 0.7
1335/0.2	95.1	6	57 ± 29	1.6 ± 0.7
1335/2	96.5	45	120 ± 58	2.2 ± 0.9
1350/2	97.3	100	119 ± 62	–

In order to determine the mechanism of fatigue failure, the silver electrodes of the fatigued specimens were removed to facilitate the observation of microstructures. The silver electrodes were first removed by grinding with silicon carbide paper and then washed with alcohol in an ultrasonic bath. Upon removing the surface electrodes, some fatigued specimens were further ground for another 50 μm with fresh silicon carbide paper and then washed again in an ultrasonic bath.

3. Results

The presence of a minor $Ba_6Ti_{17}O_{40}$ peak is detected in the XRD patterns of the $BaTiO_3$ specimens, indicating the formation of liquid phase during sintering above 1330 °C. Fig. 1 shows the typical micrographs of the $BaTiO_3$ specimens prepared for the present study. The microstructure characteristics of the specimens are listed in Table 1. Although the densities of the specimens vary within a rather narrow range (i.e., 94–97%), the amounts of coarse (i.e., abnormal) grains within the specimens vary dramatically from 0% to 100% and show a strong dependence on the sintering condition adopted. Fig. 2 shows the variation of grain size in the prepared specimens. A bimodal grain size distribution is clearly evident for the specimens sintered at 1335 °C for 2 h. In contrast, for the specimens sintered at 1350 °C for 2 h, only grains larger than 10 μm are present in the microstructure and a unimodal grain size distribution is observed.

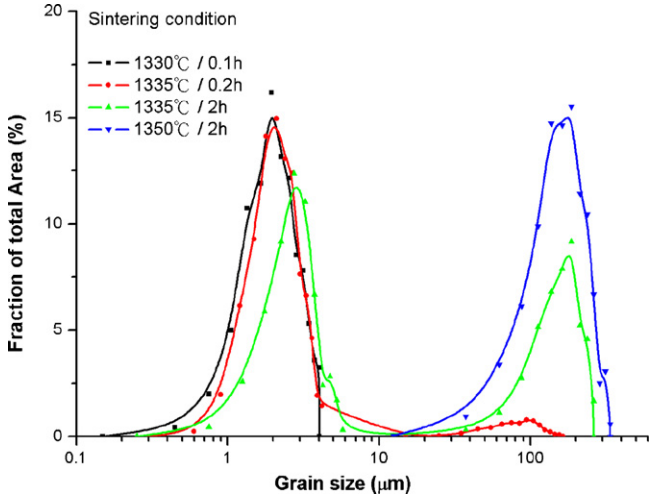

Fig. 2. Grain size distribution curves for $BaTiO_3$ specimens prepared under various sintering conditions.

Fig. 3 shows the evolution of leakage current with electric field for the prepared $BaTiO_3$ specimens. The leakage current "jumps" at certain electric field magnitudes, representing the threshold field strengths of the specimens. These threshold electric field values are treated as the dielectric breakdown strengths of the $BaTiO_3$ specimens and are summarized in Table 2. It is evident that the dielectric strength decreases with increasing sintering temperature and holding time. A period of progressive increase in leakage current before dielectric breakdown is observed for the specimen sintered at 1330 °C for 0.1 h. This behavior may be resulted from the specimen's low relative density (<94%), promoting an incremental and accumulative damage process depending on the local heterogeneities, such as the distributions of pores and grain boundary flaws.

The stable polarization *D–E* hysteresis curves for the prepared $BaTiO_3$ specimens, measured at a cyclic electric field of amplitude ±3.0 kV/mm, a frequency of 0.1 Hz and sinusoidal waveform, are shown in Fig. 4. The remanent polarization (P_r) and coercive field (E_c) values of the specimens extracted from the hysteresis curves are listed in Table 2. A significant feature regarding the microstructures of ferroelectric ceramics is that larger ceramic grains typically contain more large and stable ferroelectric domains.[17,18] It is evident from Figs. 1 and 4 that sintering conditions with higher temperature and/or longer holding time lead to an increase in grain size (or growth of coarse grains), which consequently, produce higher remanent values in polarization. The fatigue characteristics of each prepared $BaTiO_3$ specimen are examined by loading the specimen with a cyclic electric field of 1.8 kV/mm. This magnitude is smaller than the dielectric breakdown strength of the specimen

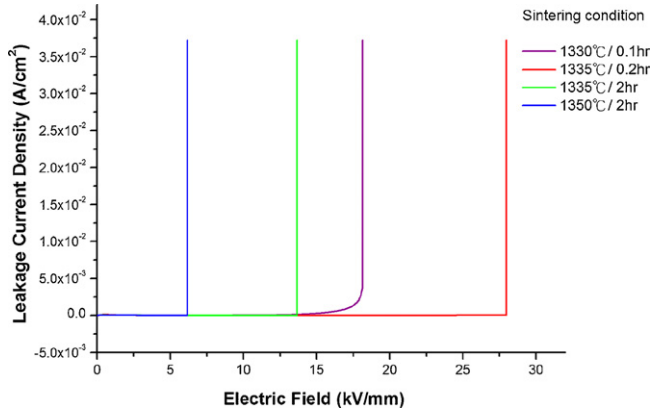

Fig. 3. Evolution of leakage current density with electric field for $BaTiO_3$ specimens prepared under various sintering conditions.

Table 2
Measured ferroelectric, breakdown and fatigue properties of $BaTiO_3$ specimens prepared under various sintering conditions.

Sintering temperature (°C)/dwell time (h)	Remanent polarization, P_r (μC/cm^2)	Coercive field, E_c (kV/mm)	Cycle number at failure	Dielectric breakdown strength (kV/mm)
1330/0.1	6.8	2.4	$>10^6$	18
1335/0.2	7.2	2.5	$>10^6$	28
1335/2	8.1	2.4	$<6 \times 10^4$	13
1350/2	11.0	3.2	$<6 \times 10^3$	6

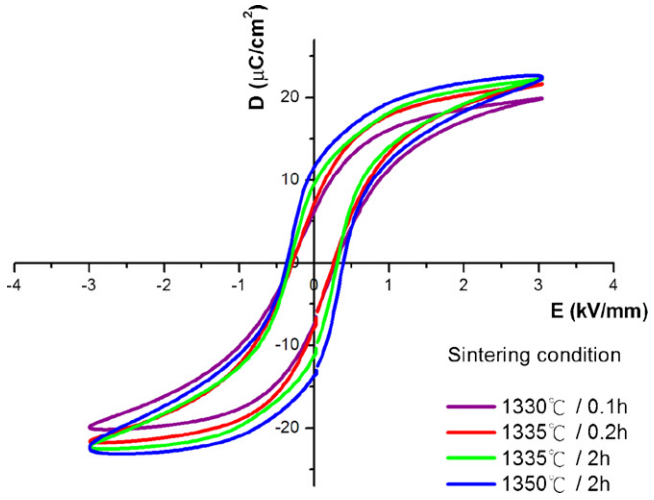

Fig. 4. Measured electric displacement D vs. electric field E hysteresis curves for $BaTiO_3$ specimens prepared under various sintering conditions (before fatiguing).

and is chosen to induce noticeable fatigue damages within one million cycles of electrical loading. In terms of degradation in resistivity, the numbers of fatigue cycles required for the specimens to exhibit a resistivity less than $10^6\ \Omega$ cm, an electrical condition in which the specimens are considered "failed" in the present study, are summarized in Table 2. For the $BaTiO_3$ specimens sintered at 1330 °C for 0.1 h and 1335 °C for 0.2 h, a resistivity less than $10^6\ \Omega$ cm has not been observed even when the fatigue loading reaches one million cycles. In contrast, the specimens sintered at 1335 °C for 2 h and 1350 °C for 2 h have failed within 10^5 cycles.

The number of cycles for failure varies not only from one type of specimen to another, but also among the same type of specimens. It is demonstrated later that the fatigue failure is resulted from the flaws within the specimens, and the variation in flaw size underlines the difference in fatigue lifetime. The Weibull approach is frequently used to characterize the flaw size distribution in brittle ceramics[19] and is adopted in the present study. The Weibull approach is based on the weakest link theory, which assumes that failure takes place at the most severe flaw in a given volume under a uniform stress. The fatigue lifetime data are presented in a format of probability of failure, F, vs. applied stress. F can be expressed as:

$$F = \frac{n - 0.5}{N} \tag{1}$$

where n is the nth specimen (specimens are ranked) and N is the total number of specimens in the batch. In the present study, stresses experienced by the specimen come from the alternating electric field. The number of cycles at failure indicates the 'survivability' of the specimen under stress. It is therefore, instead of stress, used as the parameter to quantify the fatigue failure as following:

$$\ln\left[ln\left(\frac{1}{1-F}\right)\right] = m\ \ln\ t + c \tag{2}$$

where t is the cycle number at failure, m is the Weibull modulus representing the extent of scatter, and c is the intercept in the plot of $\ln[\ln(1/(1-F))]$ vs. $\ln t$.

Fig. 5 shows the Weibull distributions for the $BaTiO_3$ specimens sintered at 1335 °C for 2 h and 1350 °C for 2 h. These two types of specimens possess the Weibull moduli of 11 and 3, respectively. For each sintering condition, 20 fatigued specimens are utilized for the Weibull analysis. It is evident from Fig. 5 that the Weibull modulus is highly influenced by the sintering condition. The coefficient of variation (i.e., standard deviation divided by average value) for the Weibull modulus depends strongly on the number of specimens adopted. As 20 fatigued specimens are used for each sintering condition, the coefficient of variation as estimated by a Monte Carlo simulation is 0.21.[20] Such a small relative variability indicates that the significant difference between the Weibull moduli of the two specimen types is genuine. Based on the cycle number at failure, the specimens sintered at 1335 °C for 2 h not only display substantially longer fatigue lifetimes than the specimens sintered at 15 °C higher, their fatigue lifetimes also vary within a much narrower range. This suggests that the $BaTiO_3$ specimens with less amount of

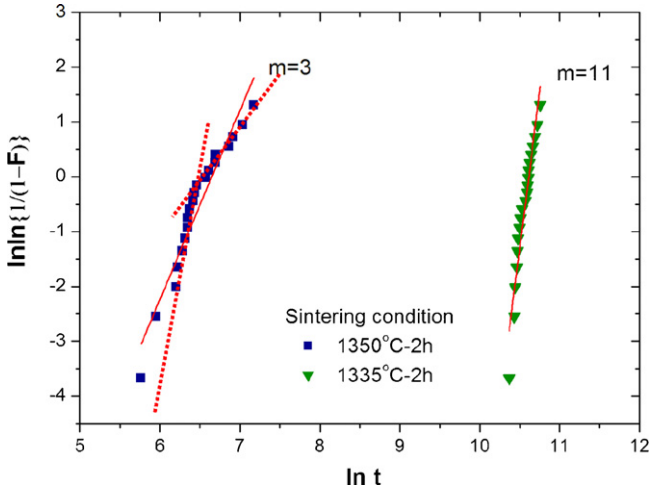

Fig. 5. Weibull distribution curves for $BaTiO_3$ specimens sintered at 1335 °C for 2 h and 1350 °C for 2 h.

Table 3
Insulation resistivity and dissipation factor of various $BaTiO_3$ specimens before and after fatigue test.

Sintering temperature (°C)/dwell time (h)	Insulation resistivity (Ω cm)		Dissipation factor	
	Before	After	Before	After
1330/0.1	10^{15}	10^{13}	0.02	0.03
1335/0.2	10^{15}	10^{13}	0.01	0.02
1335/2	10^{15}	$<10^{6}$	0.01	0.07
1350/2	10^{15}	$<10^{6}$	0.01	0.06

coarse grains have higher reliability, despite they might possess a bimodal grain size distribution.

The electrical properties of the $BaTiO_3$ specimens before and after fatiguing are summarized in Table 3. For the specimens sintered at 1330 °C for 0.1 h and 1335 °C for 0.2 h, changes in the values of resistivity and dissipation factor after 10^6 cycles of fatigue loading are relatively small. In contrast, the measured resistivity decreases more than nine orders of magnitude under similar electrical fatigue conditions for the specimens sintered at 1335 °C for 2 h and 1350 °C for 2 h. Their dissipation factors also increase by almost one order of magnitude after fatiguing, indicating a degradation in the dielectric strength.

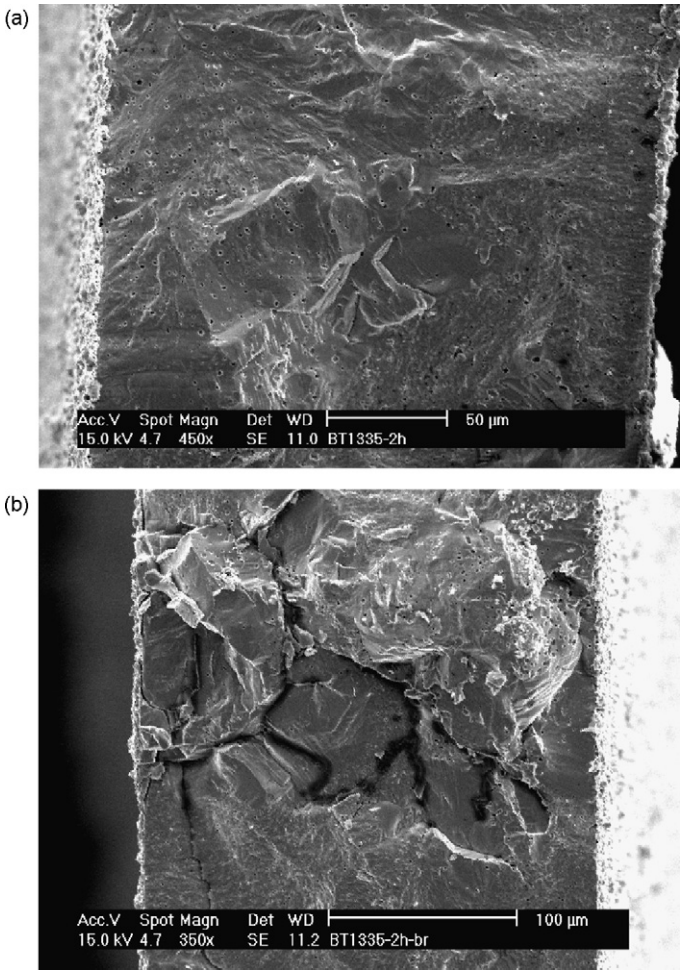

Fig. 6. Fracture surface micrographs of $BaTiO_3$ specimen (a) before and (b) after fatiguing. The specimen was sintered at 1335 °C for 2 h. Electric field-induced fatigue cracks appear black in micrograph (b).

When the fatigue test was completed, the "failed" $BaTiO_3$ specimen was subjected to a mechanical load until separation by fast fracture occurred, through the fatigue crack growth zone. This procedure allows the microstructural features at the fatigue-induced crack faces to be examined, and consequently, facilitates the identification of microstructural weak points which are commonly associated with the fatigue crack paths.[19] In the present study, although the origin of fatigue cracks on the fracture surface is difficult to identify due to the small specimen thickness, characteristic weak points in the microstructure are easily recognized based on the fatigue crack paths. A common microstructural region that is susceptible to fatigue cracking is where the coarse abnormal grains are clustered together. This is clearly demonstrated in Fig. 6. The SEM micrographs shown in Fig. 6 are the fracture surfaces of the $BaTiO_3$ specimen containing 45% abnormal grains (sintered at 1335 °C for 2 h) before and after fatiguing. The electric field-induced fatigue cracks, which appear black in the micrograph (see Fig. 6b), are predominantly intergranular and propagate through regions where the abnormal grains are interconnected to each other. The observed fatigue cracks have depths, contain random edges, and are entrenched at the grain boundaries. Due to the shadowing effects in secondary electron imaging, the fatigue cracks appear to be darker under SEM. Additionally, material burns caused by arcing within the fatigue cracks during cyclic electrical loading could alter the material composition around the cracks[4] and consequently contribute to the difference in image contrast.

Regardless of the grain size distribution, it is evident from Fig. 1 that there are no large pores and cracks present in the microstructures of the un-fatigued $BaTiO_3$ specimens. However, upon removing the silver-based electrodes from the fatigue-failed $BaTiO_3$ specimens, surface fatigue cracks are observed on the circular faces of the specimens. These cracks are still present at a depth 50 μm below the surface. The optical micrograph shown in Fig. 7 is the polished section image (50 μm below the surface) of the fatigued $BaTiO_3$ specimen containing 45% abnormal grains (sintered at 1335 °C for 2 h). When comparing Figs. 1c and 7, it is clear that the microstructure has been changed beneath the electrodes after fatiguing. Similar to the through-thickness fatigue cracks at the fracture surface, the surface fatigue cracks tend to propagate through regions where the coarse abnormal grains are clustered or along the interface between the fine and coarse grains. Large pores due to grain separations are frequently observed on the crack flanks (see Fig. 7). Within or around these large pores, deposits of elemental silver (Ag) are commonly found. Fig. 8a and b shows the deposition of Ag within and around the large pores located on the

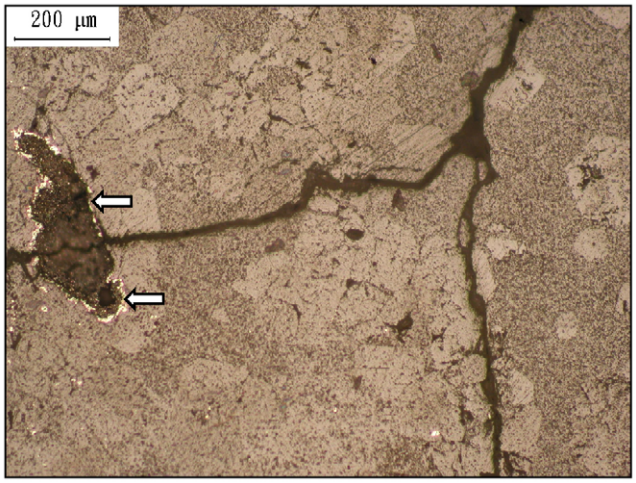

Fig. 7. Optical section image (50 μm below electrode surface) of fatigued $BaTiO_3$ specimen containing 45% abnormal grains (sintered at 1335 °C for 2 h). Large pores (arrowed) are found on crack flanks.

crack flanks, respectively. Analyses using energy dispersive X-ray spectroscopy (EDS) confirm that the deposits are indeed Ag inclusions (see Fig. 8c). Again, when comparing Figs. 1c and 8, it is clear that the Ag inclusions are not present in the microstructure before fatiguing. It is believed that the Ag inclusions come from the surface electrodes. At a depth 50 μm below the surface, the presence of Ag in the pores around the crack flanks is still evident, suggesting that elemental diffusion in the $BaTiO_3$ bulk is not the transport mechanism for Ag. It is believed that the surface electrodes "melt" toward the end of the fatigue test due to joule heating by large leakage currents. The Ag ions are then carried deep below the surface by the leakage currents via the fatigue cracks.

4. Discussion

The presence of $Ba_6Ti_{17}O_{40}$ phase in the prepared $BaTiO_3$ specimens indicates the formation of a eutectic liquid during sintering. Although the Ba/Ti ratio of the starting powder is close to unity as reported by the manufacturer, a small amount of Ba may dissolve during wet-milling and/or evaporate during sintering.[21,22] A slightly lower Ba/Ti ratio is thus resulted, and consequently, a liquid phase is formed at a sintering temperature above 1330 °C. The presence of the liquid phase can encourage the formation of abnormal grains.[12,13] Since the sintering temperature is higher than the eutectic temperature of $BaTiO_3$, the abnormal grains with equiaxed shape are therefore observed.[23] In the present study, by varying the sintering temperature from 1330 to 1350 °C and the dwell time from 0.1 to 2 h, the amount of abnormal grains in the $BaTiO_3$ specimens can be manipulated considerably. This processing approach allows us to examine the relationship between the microstructure and the dielectric and fatigue strengths. The prepared $BaTiO_3$ specimens exhibit either a single or a bimodal grain size distribution. The size of the coarse abnormal grains is nearly two orders of magnitude larger than that of the fine grains. However, the formation of the coarse abnormal grains generates microcracks at the grain

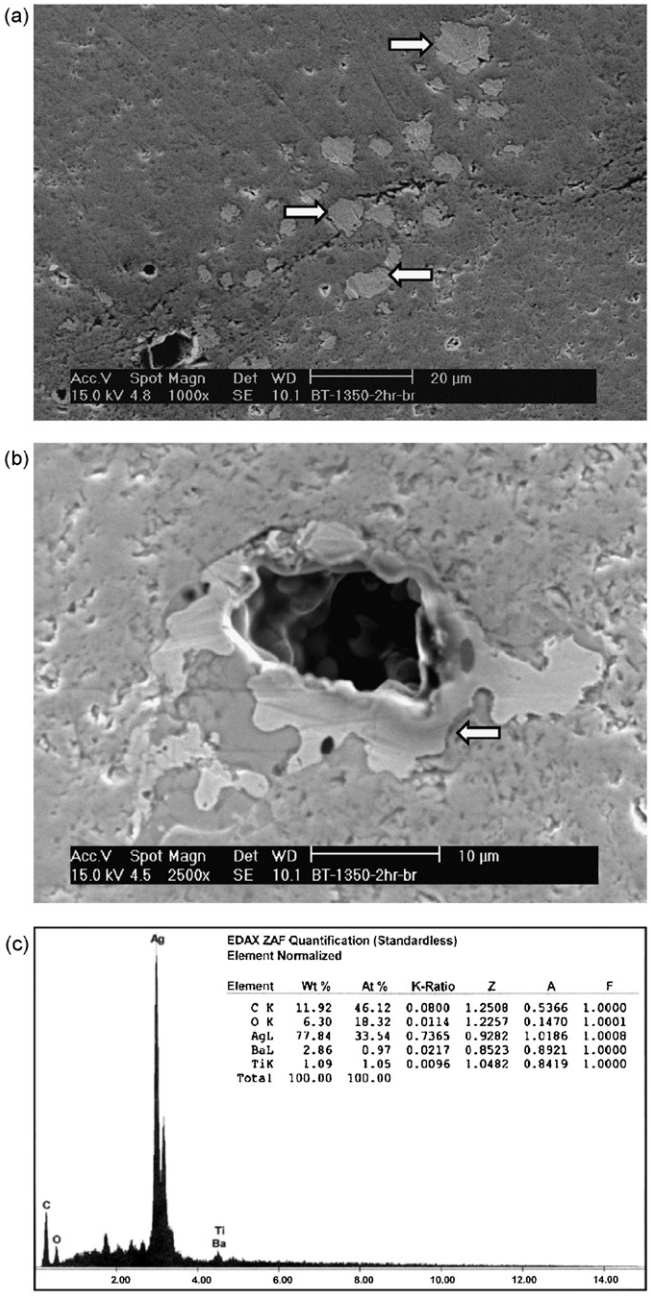

Fig. 8. SEM section micrographs showing (a) deposition of Ag within large pores (arrowed) and (b) deposition of Ag around a large pore (arrowed) located on fatigue crack flanks. (c) EDS spectrum confirming deposits within and around large pores are silver inclusions. Data shown here are those of fatigued $BaTiO_3$ specimen containing 45% abnormal grains (sintered at 1335 °C for 2 h).

boundaries. This is due to the thermal expansion anisotropy of tetragonal phase. The relationship between the presence of abnormal grains and the formation of microcracks in sintered bulk $BaTiO_3$ ceramics has been investigated and confirmed by Tuan and Lin adopting a thermal expansion analysis.[15] In this previous study, the volume expansion and shrinkage curves for the $BaTiO_3$ specimens during heating and cooling were monitored using with a dilatometer. The observed expansion and shrinkage curves were hysteretic for the $BaTiO_3$ specimens containing abnormal grains. Such hysteresis behavior indicated

a volume change due to phase transformation and was used as an evidence for the presence of microcracks in sintered bulk $BaTiO_3$ ceramics containing abnormal grains.[15]

Microstructural features shown in Figs. 6 and 7 indicate that under the influence of large alternating electric fields, the coarse grains are much more prone to fatigue failure. The amount of coarse abnormal grains in the $BaTiO_3$ specimen is therefore the governing factor in determining its dielectric and fatigue strengths. The dielectric strength decreases significantly with increasing amount of coarse grains. The fatigue strength, expressed in terms of cycle number at failure, also decreases with increasing amount of coarse grains. It is evident that the dielectric and fatigue strengths of the $BaTiO_3$ specimens depend strongly on their microstructures.

In terms of cycle number at failure, the fatigue strength of the $BaTiO_3$ specimens containing less than 5% coarse grains is longer than 10^6 cycles. As the amount of coarse grain becomes higher than 45%, the specimens reach failure criterion within 10^5 cycles. Based on the percolation theory, particles with a content higher than 45% in a system is capable of forming a continuous network[24]. The formation of abnormal grains in $BaTiO_3$ is typically accompanied with the formation of microcracks.[15] As the coarse $BaTiO_3$ grains are interconnected, the intrinsic defects are joined together forming a microstructural weak region which is highly susceptible to fatigue cracking, as clearly demonstrated in Fig. 6.

Fig. 5 indicates that the Weibull modulus of the $BaTiO_3$ specimens sintered at 1350 °C for 2 h is smaller than that of the specimens sintered at 1335 °C for 2 h. Upon examining the scatters in the coarse grain size of these two types of specimens, it is found that the size distribution of the coarse grains (i.e., the right-hand side peak of the distribution curve shown in Fig. 2) is wider for the specimens sintered at 1350 °C for 2 h. A wider scatter in the coarse grain size gives rise to a lower Weibull modulus. The Weibull line obtained for the specimens sintered at 1350 °C for 2 h is consisted of two sections with different slopes (indicated by the two dotted lines in Fig. 5). One section indicates a short fatigue lifetime with a high Weibull modulus, while the other section shows a long fatigue lifetime with a low Weibull modulus. The presence of two slope sections in the Weibull line implies the presence of two different failure mechanisms. This might be attributed to the wide scatter in the size of the coarse abnormal grains. Further investigations based on thorough microstructure characterizations of the fatigued $BaTiO_3$ specimens with various types of grain size distributions should reveal clearer details.

5. Conclusions

In the present study, the effect of the amount of coarse abnormal grains on the dielectric and fatigue strengths of bulk $BaTiO_3$ ceramics is studied. By varying the sintering temperature from 1330 to 1350 °C and the dwell time from 0.1 to 2 h, the amount of coarse grains in the $BaTiO_3$ specimens can be manipulated considerably. Fatigue data under cyclic electrical loading are presented for the $BaTiO_3$ specimens of different grain size distributions. Both the dielectric and fatigue strengths decrease significantly with increasing amount of coarse grains. Based on the Weibull analyses, it is concluded that a wider scatter in the coarse grain size gives rise to a lower Weibull modulus, and $BaTiO_3$ ceramics with less amount of coarse grains have higher reliability, despite they might possess a bimodal grain size distribution. Characteristic weak points in the microstructure are recognized based on the fatigue crack paths. A common microstructural region which is susceptible to fatigue cracking is where the coarse abnormal grains are clustered together. The electric field-induced fatigue cracks are predominantly intergranular and propagate through regions where the abnormal grains are interconnected to each other. The formation of coarse abnormal grains in $BaTiO_3$ is typically accompanied with the formation of microcracks. The clustering of the coarse grains joins the intrinsic defects, and consequently, forming a microstructural weak region. The present study demonstrates that the dielectric and fatigue strengths of bulk $BaTiO_3$ ceramics depend strongly on their microstructures.

Acknowledgements

The present work is supported by the National Science Council, Taiwan, through contract number of NSC97-2221-E-002-030.

References

1. Kishi H, Mizuno Y, Chazono H. Base-metal electrode-multilayer ceramic capacitors: past, present and future perspectives. *Jpn J Appl Phys* 2003;**42**:1–15.
2. Garcia V, Fusil S, Bouzehouane K, Enouz-Vedrenne S, Mathur ND, Barthelemy A, et al. Giant tunnel electroresistance for non-destructive readout of ferroelectric states. *Nature* 2009;**460**:81–4.
3. Jiang Q, Cao W, Cross LE. Electric fatigue in lead zirconate titanate ceramics. *J Am Ceram Soc* 1994;**7**:211–5.
4. Shieh J, Huber JE, Fleck NA. Fatigue crack growth in ferroelectrics under electrical loading. *J Eur Ceram Soc* 2006;**26**:95–109.
5. Cao H, Evans AG. Electric-field-induced fatigue crack growth in piezoelectrics. *J Am Ceram Soc* 1994;**77**:1783–6.
6. Lynch CS, Chen L, Yang W, Suo Z, McMeeking RM. Crack growth in ferroelectric ceramics driven by cyclic polarization switching. *J Intell Mater Syst Struct* 1995;**6**:191–8.
7. Qian R, Lukasiewicz S, Gao Q. Electrical fatigue response for ferroelectric ceramics under electrical cyclic load. *Solid-State Electron* 2000;**44**:1717–22.
8. Weitzing H, Schneider GA, Steffens J, Hammer M, Hoffmann MJ. Cyclic fatigue due to electric loading in ferroelectric ceramics. *J Eur Ceram Soc* 1999;**19**:1333–7.
9. Nuffer J, Lupascu DC, Rödel J. Damage evolution in ferroelectric PZT induced by bipolar electric cycling. *Acta Mater* 2000;**48**:3783–94.
10. Fang DN, Liu B, Sun CT. Fatigue crack growth in ferroelectric ceramics driven by alternating electric fields. *J Am Ceram Soc* 2004;**87**:840–6.
11. Westram I, Laskewitz B, Lupascu DC, Kamlah M, Rödel J. Electric-field induced crack initiation from a notch in a ferroelectric ceramic. *J Am Ceram Soc* 2007;**90**:2849–54.
12. Hennings DFK, Janssen R, Reynen PJL. Control of liquid-phase-enhanced discontinuous grain growth in barium titanate. *J Am Ceram Soc* 1987;**70**:23–7.
13. Rios PR, Yamamoto T, Knodo T, Sakuma T. Abnormal grain growth kinetics of $BaTiO_3$ with an excess TiO_2. *Acta Mater* 1998;**46**:1617–23.
14. Schneider GA, Heyer V. Influence of the electric field on Vickers indentation crack growth in BaTiO3. *J Eur Ceram Soc* 1999;**19**:1299–306.

15. Tuan WH, Lin SK. The microstructure–mechanical properties relationships of BaTiO3. *Ceram Int* 1999;**25**:35–40.
16. Chen YH, Lu SC, Tuan WH, Chen CY. Microstructure transition from normal to abnormal grains for $BaTiO_3$. *J Eur Ceram Soc* 2009;**29**:3243–8.
17. Jona F, Shirane G. *Ferroelectric crystals*. Oxford: Pergamon Press; 1962.
18. Lines ME, Glass AM. *Principles and applications of ferroelectrics and related materials*. Oxford: Clarendon Press; 1977.
19. Weibull W. A statistical distribution function of wide applicability. *J Appl Mech* 1951;**18**:293–8.
20. Ritter JE, Bandyopadhyay N, Jakus K. Statistical reproducibility of the dynamic and static fatigue experiments. *Am Ceram Soc Bull* 1981;**60**:798–806.
21. Chiang CW, Jean JH. Effects of barium dissolution on dispersing aqueous barium titanate suspensions. *Mater Chem Phys* 2003;**80**:647–55.
22. Chun JS, Hwang NM, Kim DY. Abnormal grain growth occurring at the surface of a sintered $BaTiO_3$ specimen. *J Am Ceram Soc* 2004;**87**:1779–81.
23. Lee BK, Chung SY, Kang SJL. Grain boundary faceting and abnormal grain growth in $BaTiO_3$. *Acta Mater* 2000;**48**:1575–80.
24. McLachlan DS, Newnham RE. Electrical resistivity of composites. *J Am Ceram Soc* 1990;**73**:2187–203.